Molecular Determinant for Specific Ca/Ba Selectivity Profiles of Low and High Threshold Ca^{2+} Channels

Thierry Cens,[1,2] Matthieu Rousset,[1,2] Andrey Kajava,[1,2] and Pierre Charnet[1,2]

[1]Centre de Recherche de Biochimie Macromoléculaire, UMR 5237 Centre National de la Recherche Scientifique, 34293 Montpellier, France

[2]University of Montpellier II, 34095 Montpellier, France

Voltage-gated Ca^{2+} channels (VGCC) play a key role in many physiological functions by their high selectivity for Ca^{2+} over other divalent and monovalent cations in physiological situations. Divalent/monovalent selection is shared by all VGCC and is satisfactorily explained by the existence, within the pore, of a set of four conserved glutamate/aspartate residues (EEEE locus) coordinating Ca^{2+} ions. This locus however does not explain either the choice of Ca^{2+} among other divalent cations or the specific conductances encountered in the different VGCC. Our systematic analysis of high- and low-threshold VGCC currents in the presence of Ca^{2+} and Ba^{2+} reveals highly specific selectivity profiles. Sequence analysis, molecular modeling, and mutational studies identify a set of non-conserved charged residues responsible for these profiles. In HVA (high voltage activated) channels, mutations of this set modify divalent cation selectivity and channel conductance without change in divalent/monovalent selection, activation, inactivation, and kinetics properties. The $Ca_V2.1$ selectivity profile is transferred to $Ca_V2.3$ when exchanging their residues at this location. Numerical simulations suggest modification in an external Ca^{2+} binding site in the channel pore directly involved in the choice of Ca^{2+}, among other divalent physiological cations, as the main permeant cation for VGCC. In LVA (low voltage activated) channels, this locus (called DCS for divalent cation selectivity) also influences divalent cation selection, but our results suggest the existence of additional determinants to fully recapitulate all the differences encountered among LVA channels. These data therefore attribute to the DCS a unique role in the specific shaping of the Ca^{2+} influx between the different HVA channels.

The Journal of General Physiology

INTRODUCTION

Low (LVA = $Ca_V3.1$-3) and high (HVA = $Ca_V1.1$-4, $Ca_V2.1$-3) threshold voltage-gated Ca^{2+} channels, by allowing selective, rapid, and large Ca^{2+} influx into cells, are key actors of the Ca^{2+} homeostasis (Isom et al., 1994; Catterall, 2000) and thus play a fundamental role in cell physiology by activating a myriad of Ca^{2+}-driven processes. Although channel-specific gating, localization, regulation, and protein partners finely tune this Ca influx and thus directly participate in the precise channel physiological or pathophysiological roles, the key feature that makes these channels so important is undoubtedly their capacity to select Ca^{2+} ions among other physiological monovalent and divalent cations. The channel preference for Ca^{2+} versus the monovalent Na^+ has been the subject of a number of studies (Sather et al., 1994; Varadi et al., 1999; Cibulsky and Sather, 2003; Sather and McCleskey, 2003) mostly performed on the prototypal HVA $Ca_V1.2$ channels with only sparse data available on other channel types (Serrano et al., 2000; Talavera et al., 2001; Sather and McCleskey, 2003).

The mechanism of Ca^{2+} ion selection and permeation relies on the pore-forming $Ca_V\alpha$ subunit. $Ca_V\alpha$ subunits are composed of four domains, each containing six transmembrane segments and a pore-forming loop (P loop), arranged around a pseudo-symmetrical axis forming a central pore. Theoretical analysis and experimental finding, performed on $Ca_V1.2$ channels, have suggested that the basis of selection and high transfer rate of Ca^{2+} ions relies on direct interactions of two ions with specific residues in the pore (Hess and Tsien, 1984; Varadi et al., 1999; Sather and McCleskey, 2003). Molecular studies identified a single site, the EEEE (EEDD in LVA channels) locus, constituted by a ring of four glutamates (2E + 2D in LVA channels) located at equivalent position in each of the P loop of the four domains (* in Fig. 2), and responsible for the multi-ionic nature of the Ca^{2+} channel pore (Heinemann et al., 1992; Kim et al., 1993; Tang et al., 1993; Yang et al., 1993; Ellinor et al., 1995; Cibulsky and Sather, 2000). The binding of one or two Ca^{2+} ions in the EEEE locus can explain the apparent antagonism between high permeability and high selectivity typical of these Ca^{2+} channels (Sather and McCleskey, 2003). However several studies indicate VGCC-specific selectivities for divalent cations with Ca/Ba

Correspondence to Pierre Charnet: pierre.charnet@crbm.cnrs.fr

The online version of this article contains supplemental material.

Abbreviations used in this paper: AMFE, anomalous mole fraction effect; DCS, divalent cation selectivity; HVA, high voltage–activated; LVA, low voltage–activated; VGCC, voltage-gated Ca^{2+} channels.

permeability ratios varying from 0.3 to 1.2 for $Ca_V1.2$ and $Ca_V2.3$ for example (Bourinet et al., 1996), suggesting that the choice of Ca^{2+}, crucial for cell physiology, cannot be explained by this conserved EEEE locus. Other motifs known to contribute to channel permeation (Feng et al., 2001) are conserved among HVA channels and thus are not good candidates to explain channel-specific properties. Furthermore, mutation of the two Asp present at the EEDD locus of all LVA channels to Glu, as in HVA, cannot bestow HVA-like selectivity profiles (Talavera et al., 2001). Clearly, additional mechanisms and/or loci may exist to fully explain Ca^{2+} selection.

We have performed the first analysis of the relative permeability of Ba^{2+} and Ca^{2+} ions of three LVA and four HVA VGCCs expressed in *Xenopus* oocytes. Specific permeation profiles are detected for each channel by characterizing the anomalous mole fraction effect (AMFE). Inspection of the amino acid sequences of these channels in the pore region reveals a novel and channel-specific locus composed of nonconserved charged residues. In HVA channels, modifications of this site strongly influence the Ba^{2+}/Ca^{2+} permeability ratio without modifying the monovalent/divalent selection and the sensitivity to Cd^{2+} block. Our results, completed with numerical simulation and molecular modeling, suggest that this set of amino acids (thereafter called DCS [divalent cation selection]), is located in the upper halve of the channel and points toward the pore, where it may form a second Ca^{2+} binding site. In LVA channels, mutation of the DCS also influences channel selectivity, although additional sites clearly exit. DCS is present in all VGCC and is crucial for the definition of their specific permeability profile, and thus for Ca^{2+} entry into cells.

MATERIALS AND METHODS

Molecular Biology

Mutations in rat brain $Ca_V2.1$ and $Ca_V2.3$ were introduced by PCR (GenBank/EMBL/DDBJ accession nos. M64372 and L15453, respectively). Mutations $T_{264}D$, $T_{264}A$, $T_{264}G$, $E_{612}S$, $E_{612}A$, $E_{612}G$, $G_{1323}F$, $Q_{1328}E$, $Q_{1328}A$, $Q_{1328}G$, $S_{1611}C$, $E_{1619}N$, $E_{1619}A$, $E_{1619}G$, $E_{1619}D$, and $QE_{1618\text{-}1619}HN$ were introduced by PCR mutagenesis into the rbEII sequence ($Ca_V2.3$, GenBank/EMBL/DDBJ accession no. 15453). PCR fragments were then subcloned into a modified version of the pBluescript cloning vector, using native (NotI, XbaI, Bst98I, ApaI, HindIII, XhoI) or created (Mlu(1007), KpnI(polylinker)) restriction sites, and fully sequenced. Full-length cDNA was constructed by ligating appropriate fragments. Mutations are written explicitly in the text. The same approach has been followed to construct $Ca_V2.1$(TEQE) (rbAI, M64373). In this case, an additional mutation (histidine at position −1, referred to the DCS locus, into glutamine) was also made to preserve the pore structure of $Ca_V2.3$ (see Fig. 2). The reverse mutation (Q to H) was made on the $Ca_V2.3$ (DEQN). Finally, $Ca_V2.3$, $Ca_V2.1$, $Ca_V1.2$ (M67515), $Ca_V\beta2a$ (M80545), and $Ca_V\alpha2\text{-}\delta$ (M86621) were subcloned into the pMT2 expression vector for oocyte injection and expression.

Electrophysiology

Isolated *Xenopus laevis* oocytes were injected with a mixture of plasmids encoding the $\alpha_2\text{-}\delta + \beta_2$ and each of the mutant $Ca_V2.1$ or $Ca_V2.3$ Ca^{2+} channel subunits at a total DNA concentration of 0.2 μg/μl. LVA $Ca_V3.1$, $Ca_V3.2$, and $Ca_V3.3$ subunits were injected alone. Total whole-cell currents were recorded under two-electrode (resistance: 0.5–1 MΩ in 3 M KCl) voltage-clamp (geneclamp 500; Axon Instruments Inc.) using solutions of increasing Ca^{2+} mole fraction (in mM: BaOH/CaOH, 10/0, 9/1, 8/2, 6/4, 4/6, 2/8, 0/10; TEAOH, 20; CsOH, 2; NMDG, 50; HEPES, 10, pH set to 7.2 using methane sulfonic acid). Voltage ramps from −80 to +80 mV (at 0.4 V/s) or −100 mV to +60 mV (at 0.4 to 2.6 V/s) were applied every 15 s on HVA or LVA VGCC–expressing oocytes, respectively. The speed of the ramp was chosen after experimental testing to minimize the error in the current–voltage curve when channel inactivation was fast ($Ca_V3.1$, $Ca_V3.2$). Oocytes were injected with 40 nl of a 100 mM BAPTA solution to block contaminating Ca^{2+}-activated Cl current. In Fig. 5, the extent of AMFE was quantified by dividing the minimum of the current–mole fraction curve by the current recorded at 10 mM Ca^{2+}. This allowed us to visualize the presence of AMFE (values <1) and the extent of the Ca/Ba current ratio on the same graph. This is not valid for channels without AMFE and with Ca^{2+} current larger than Ba currents, a case not present in HVA channels. The correlation between the number of charges and the extent of AMFE was tested using the Spearman correlation test at the 0.05 level.

Single-channel recordings were obtained in cell-attached patch with a bath solution composed of (in mM) 100 KCl, 2 $MgCl_2$, 10 HEPES, 10 EGTA; pH set to 7.4 using KOH. The pipettes (10–20 MΩ) were filled with (in mM) 100 $BaCl_2$, 10 HEPES; pH set to 7.2 using NaOH. Currents were filtered at 2 kHz and digitized at 10 kHz. Channel conductances were calculated from linear regressions of single channel amplitudes obtained at different pipette voltages and determined using idealized event histograms (Clampfit, version 9.0, Axon Instruments Inc.). All values are presented as mean ± SEM. Bay-K 8644 (1 μM) was added to the pipette solution for the recordings obtained on the $Ca_V1.2$ channels.

Molecular Modeling

The helices P and S6 being located in the hydrophobic interior of the structure have highly apolar sequences and are connected by a variable hydrophilic link. This motif was identified in each of four Ca^{2+} channel domains and aligned with the sequence of KvAT by using CLUSTALW program (Higgins et al., 1996). The sequence alignment was then manually corrected whenever necessary based on the available crystal structure of the K^+ channel (Jiang et al., 2003). The structure of the K^+ channel provides several constraints that we used to model the 3D structure of Ca^{2+} channel. The C-terminal ends of four P helices come in direct contact in the tetramer center. This arrangement requires a perpendicular exit from the α-helical C-terminal cap (Efimov, 1993) induced by the lefthanded α-helical conformation of Thr196. In the alignment that was used for the modeling, the hydrophobic region of the Ca^{2+} channel corresponding to the P helix is frequently followed by glycine (methionine in domain I). Glycine following the α-helix in the lefthanded α-helical conformation is the typical case of the perpendicular exit from the α-helix (Efimov, 1993). Therefore, these glycines were aligned with Thr196 of KvAT. The next five residues represent a pore-lining region (pink bar in Fig. S2 B, available at http://www.jgp.org/cgi/content/full/jgp.200709771/DC1). In the alignment, the residues of the EEEE and DCS loci of the Ca^{2+} channel are within the pore-lining region. Furthermore, an aromatic Tyr199 of the K^+ pore-lining region that faces the hydrophobic interior of the structure (marked by an arrow in Fig. S2 B) is aligned with the conserved aromatic tryptophans of the Ca^{2+} channel. The following loop between the pore-forming region and α-helix S6 moves away from the pore

and can be variable (broken line on Fig. S2 B). Therefore, in the sequence alignment these regions are hydrophilic and of different length. The initial model containing helices P and S6 was built by using the HOMOLOGY module of InsightII program (Dayring et al., 1986) and the alignment shown on Fig. S2 B. Then the pore-lining region of the Ca^{2+} channel was modeled manually taking into consideration the following constraints: (a) all four loops have the same backbone conformation, (b) the side chains of the EEEE and DCS loci are directed toward the Ca^{2+} ions, as suggested by effects of the mutations, and (c) the aromatic tryptophans occupy the same hydrophobic pocket of the helices P and S6 as the aromatic Tyr199 in the K^+ channel. The conformational analysis showed that to meet all these conditions the pore-lining region of the Ca^{2+} channel requires a conformation that is different from one of the K^+ channel. In our model (Fig. 2 B), this region has a conformation of the polyproline helix instead of an alternation of lefthanded and righthanded α-helical conformations observed in the K^+ channel. Two Ca^{2+} ions were introduced in the EEEE and DCS locus, and side chains of the locus were manually adjusted to coordinate the cations. The final structure was energy minimized using InsightII program (Dayring et al., 1986). The energy minimization and molecular dynamics calculations of our model suggested that the side chains of the EEEE locus coordinating Ca^{2+} are packed tighter than the ones of the DCS locus and this can be explained by the higher affinity of the EEEE site. The superposition of the energy-minimized Ca^{2+} channel model with the structure of K^+ channel shows that the subunits of Ca^{2+} channel move away from the center of the pore to allow the side chains of EEEE locus to accommodate the pore.

Numerical Simulation

The two binding-site model for calcium channels was essentially derived from (Begenisich and Cahalan, 1980; Hess and Tsien, 1984; Campbell et al., 1988; Kurata et al., 1999) with minor changes in the energy profiles to account for the specific permeation properties of $Ca_V2.3$. The energy profile of LVA channels was obtained from that of $Ca_V2.3$ by slight adjustment of the binding energy of the internal well (the EEEE/EEDD locus) to provide current traces compatible with $Ca_V3.1$ currents. These two profiles served then as references and all subsequent computations were made by varying only the binding energy of the first extracellular well (DCS locus) that was supposed to be modified by the mutations. The three energy peaks (P1, P2, P3) and the two wells (DCS and EEE) were regularly spaced within the membrane at similar electrical distances (Rosenberg and Chen, 1991). The membrane potential (Vm) is supposed to fall across the narrow region of the pore. The rate constants for the transitions between the different channel states were calculated by Eyring rate theory as rate = $kT/h \exp(-\Delta G)$, where ΔG is the sum of the chemical energy, given by the energy differences between the peak and the well, the electric energy, given by the movement of the cation through the electrical field (zVm/d; d electrical distance), and an electrostatic repulsive force due to occupancy of two binding sites by two cations ($z_i z_j \ln(F)$) (see Begenisich and Cahalan, 1980; Hess and Tsien, 1984; Campbell et al., 1988; Kurata et al., 1999). The energy profiles for Ca^{2+} and Ba^{2+} were (in RT units) 4, −19.8, −7.5, −17.5, 5 and 4, −17.4, 1, −15.5, 5.2 for LVA and 4, −19.5, −7.5, −18.1, 1 and 4, −14.5, 1, −14.7, 2 for HVA channels. Extracellular and intracellular total divalent cation concentrations were set to 10 mM and 0.1 μM, respectively. Computation of steady-state ionic currents at different Ca^{2+} mole fractions and decreasing DCS locus energy (−20 to −12 RT units) was made by using the matrix inversion method to solve the nine differential equations of the occupancy probabilities for the nine possible states of the model. ICa/IBa was computed as the ratio of the currents calculated in 10 mM pure Ca^{2+} and Ba^{2+}, respectively. The program was written using Matlab (The Mathworks Inc.).

Online Supplemental Material

The online supplemental material is available at http://www.jgp.org/cgi/content/full/jgp.200709771/DC1. Tables S1–S3 show voltage-dependent properties of $Ca_V2.1$ and $Ca_V2.3$ mutant channels. Fig. S1 shows comparative analysis of ramp versus step voltage to record AMFE. Fig. S2 is a compilation of the selective permeation profile and amino acid alignment of the pore region of $Ca_V2.3$ and Kv channels. Fig. S3 shows activation and inactivation curves of $Ca_V2.1$ and $Ca_V2.3$ mutant channels. Fig. S4 shows the effect of non-DCS mutations on AMFE.

RESULTS

One of the major theoretical outcomes of the two Ca^{2+} binding-site model for Ca^{2+} channel permeation is the presence of AMFE, where, in the presence of mixtures of Ba^{2+} and Ca^{2+} ions at a total constant concentration, the measured peak current–mole fraction curve is nonmonotonic and goes through a minimum (Hess and Tsien, 1984). AMFE was first described for L-type VGCC (Almers et al., 1984; Hess and Tsien, 1984). AMFE was also later reported for P/Q-type $Ca_V2.1$ channels (Mangoni et al., 1997) and expected to be very weak, from theoretical considerations, in $Ca_v3.1$ channels (Serrano et al., 2000). However, a complete comparative analysis of the Ba/Ca selectivity and AMFE of all LVA and HVA channels has never been done.

Current–voltage curves were recorded on *Xenopus* oocytes expressing different LVA and HVA VGCC under extracellular ionic conditions that allowed the detection of AMFE and the characterization of the Ba/Ca permeability. As shown on the current traces recorded during voltage ramps in the presence of 10/0, 9/1, 8/2, 6/4, 4/6, 2/8, and 0/10 Ba/Ca mole fractions (total cation concentration kept constant at 10 mM), L-type ($Ca_V1.2$), P/Q-type ($Ca_V2.1$), N-type ($Ca_V2.2$), but also R-type ($Ca_V2.3$) HVA Ca^{2+} channels displayed a marked AMFE, with a characteristic (and statistically significant) minimum peak current value for low Ca^{2+} mole fractions (current traces and peak current–Ba/Ca mole fraction curves are shown in Fig. 1, A and C). These channels nevertheless displayed different relative amplitudes of their Ca^{2+} and Ba^{2+} currents at 10 mM (ICa/IBa), ranging from 0.31 ± 0.01 (n = 23) for $Ca_V1.2$, 0.41 ± 0.02 (n = 8) for $Ca_V2.2$, and 0.51 ± 0.02 (n = 17) for $Ca_V2.1$ to 1.12 ± 0.03 (n = 13) for $Ca_V2.3$ (Fig. 1 C), suggesting specific permeation profiles despite conserved EEEE locus. Similar results were also found when current–voltage curves were obtained from voltage steps instead of voltage ramps, demonstrating that these differences were not due to differences in Ca^{2+}-dependent inactivation among the different VGCC (Fig. S1, available at http://www.jgp.org/cgi/content/full/jgp.200709771/DC1).

Surprisingly, when LVA T-type $Ca_V3.1$, $Ca_V3.2$, or $Ca_V3.3$ VGCC were expressed in oocytes and submitted to the same experimental protocol (Fig. 1, B and C),

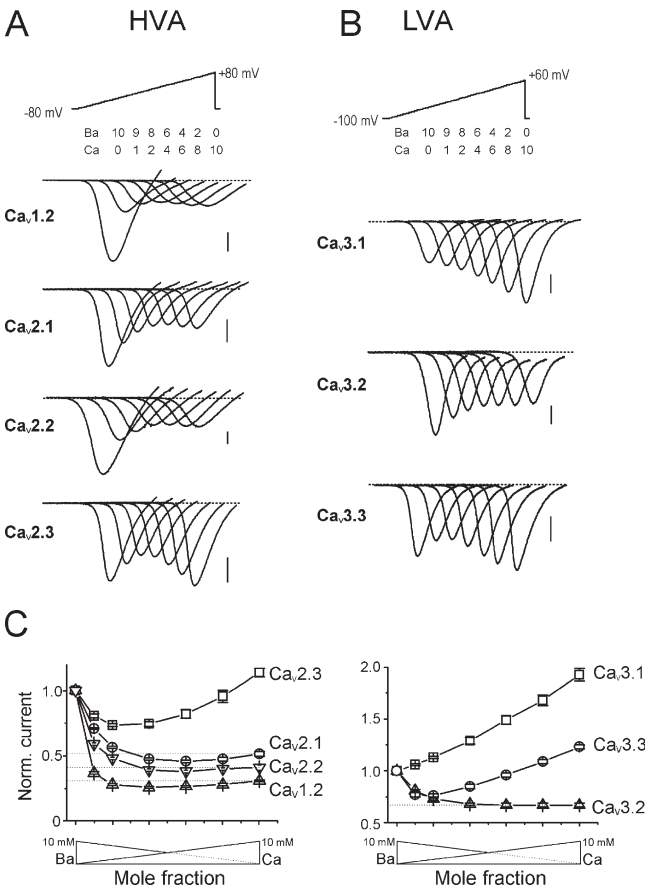

Figure 1. Low and high voltage–activated Ca^{2+} channels have specific Ca^{2+}/Ba^{2+} selectivities. (A and B) Representative current traces recorded in oocytes expressing HVA $Ca_V1.2$, $Ca_V2.1$, $Ca_V2.2$, or $Ca_V2.3$ and $\alpha_2\delta + \beta_2$ Ca^{2+} channel subunits (A) or LVA $Ca_V3.1$, $Ca_V3.2$, or $Ca_V3.3$ Ca^{2+} channels (B) using solutions of different Ca^{2+} mole fractions (Ba^{2+}/Ca^{2+}: 10/0, 9/1, 8/2, 6/4, 4/6, 2/8, and 0/10 mM). Whole-cell currents were recorded during voltage ramps from −80 to +80 mV (A) or from −100 to +60 mV (B) at a speed of 0.4 to 2.6 V/s applied every 15 s. Bars, 100 nA. (C) Normalized current/mole fraction curves obtained from recordings similar to those in A or B by plotting the peak current of the IV curve against the Ca/Ba mole fraction. Note the different ICa/IBa ratios and the presence/absence of AMFE in each case. Left, averaged curves obtained from oocytes expressing $Ca_V1.2$ (△), $Ca_V2.1$ (○), $Ca_V2.2$ (▽), or $Ca_V2.3$ (□) HVA VGCC. Right, curves obtained from oocytes expressing $Ca_V3.1$ (□), $Ca_V3.2$ (△) or $Ca_V3.3$ (○) LVA VGCC.

AMFE was only recorded for $Ca_V3.3$, while peak current decreased, or increased, monotonically with increasing Ca^{2+} mole fractions for $Ca_V3.2$ and $Ca_V3.1$ channels, respectively. These new results were completely unexpected since these three channels display the same sequence at their EEDD locus. Moreover, all three channels display a specific Ba/Ca permeability with either larger (ICa/IBa = 1.91 ± 0.06, n = 10, for $Ca_V3.1$), smaller (ICa/IBa = 0.67 ± 0.02, n = 8, for $Ca_V3.2$), or similar (1.23 ± 0.02, n = 5, for $Ca_V3.3$) Ca^{2+} currents relative to Ba^{2+} currents.

When compiled together, these data unambiguously underlined channel-specific permeation profiles in the two channel families (see Fig. S2 A). Such a specificity cannot be explained by the only high-affinity Ca^{2+} binding site identified, which is perfectly conserved in these two families (the EEEE and EEDD loci in HVA and LVA channels, respectively, see * box in Fig. 2 A) (Cibulsky and Sather, 2000; Sather and McCleskey, 2003). Inspection of the aligned amino acid sequences (Fig. 2 A) of the pore-forming P loops of HVA and LVA channels reveals the existence of a single set of nonconserved negatively charged residues located at a homologous position in each of the four domains of the $Ca_V\alpha$ subunits, four residues upstream of the well-characterized EEEE/EEDD locus (# box in Fig. 2 A). This DCS locus comprises amino acids DSED, DEQN, DAME, and TEQE in the channel domains I–IV, respectively, in $Ca_V1.2$, $Ca_V2.1$, $Ca_V2.2$, and $Ca_V2.3$ and amino acids DKDG, DVNG, and EVNG in $Ca_V3.1$, $Ca_V3.2$, and $Ca_V3.3$ channels.

The lack of structural data on the pore of the VGCC imposed the use of molecular modeling to visualize the possible arrangement of the four $Ca_V2.3$ P loops at the EEEE and DCS loci. This exercise has been done using voltage-gated K^+ channel as template (Doyle et al., 1998; Jiang et al., 2003) with major constraints that take into account the fundamental differences that exist between the K^+ and Ca^{2+} channel pores; see Fig. 2 B and Fig. S2 B (Hille, 2001; Lipkind and Fozzard, 2001). The DCS locus is located on the extracellular side of the EEEE locus but likely within the membrane electric field as suggested (Hess and Tsien, 1984) and with interloci distances of ∼8 Å. The carboxyl oxygens of the DCS locus can point toward the channel lumen, allowing their participation in the coordination of incoming divalent cations. Thus, from theoretical and experimental consideration on AMFE, the DCS locus constitutes, in several respects, a good candidate for a specific role in divalent cation selection.

Although all residues at this locus may not play an equivalent role, as is the case at the EEEE locus (Kim et al., 1993; Mikala et al., 1993; Tang et al., 1993; Yang et al., 1993; Parent and Gopalakrishnan, 1995; Cloues et al., 2000), our first hypothesis was that the total number of negatively charged residues at this location was critical for the binding of Ca^{2+} ions.

To test this hypothesis, 19 mutations were engineered in the DCS locus of $Ca_V2.3$, where the number of negatively charged residues was either increased (DSEE, DSED, and DEEE) or decreased (TSQN, GGGG, and AAAA). The resulting six mutants, labeled $Ca_V2.3$(DSEE), $Ca_V2.3$(DSED), $Ca_V2.3$(DEEE), $Ca_V2.3$(TSQN), $Ca_V2.3$(GGGG), and $Ca_V2.3$(AAAA), respectively (Fig. 3), were tested for their effect on channel selectivity. Currents recorded from *Xenopus* oocytes injected with the $Ca_V2.3$ (DSED) mutant cDNA showed a marked minimum for Ba/Ca mixtures of low Ca^{2+} mole fractions, and pure Ca^{2+} currents were clearly smaller than pure Ba^{2+} currents

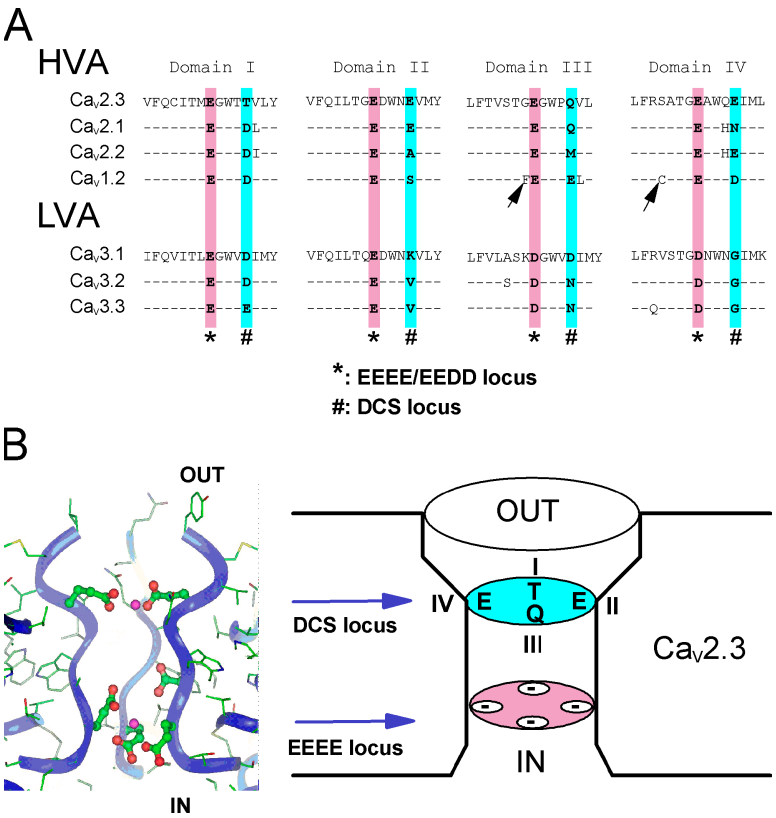

Figure 2. Molecular modeling of the DCS and EEEE loci in the channel pore. (A) Sequence alignment of the P loops of $Ca_V1.2$, $Ca_V2.1$, and $Ca_V2.3$ HVA channels and $Ca_V3.1$, $Ca_V3.2$, and $Ca_V3.3$ LVA channels. * and # boxes, position of EEEE and DCS loci in each domain of the $Ca_V\alpha$ subunit. Note the nonconservation of the DCS charged amino acids. Arrows underline the non-DCS amino acids mutated in Fig S4: S1611 and G1323 in $Ca_V2.3$. (B) A molecular model of the C-terminal end of the four P loops of $Ca_V2.3$ channel. Left, radial projection of the channel with one of the domains omitted for the clearness of the picture. Right, schematic representation of the EEEE and DCS loci of $Ca_V2.3$ channel. Ribbons represent the backbone of the peptidic chains. Ca^{2+} ions are shown as magenta balls. Negatively charged side chains of the channel are shown by ball-and-stick representation (see Materials and methods for details).

(ICa/IBa = 0.60 ± 0.05, n = 16, circle, Fig. 3, A and B). This type of behavior was typical of $Ca_V1.2$ channels, which also possessed three negative charges at the DCS locus. Similar results were also found with the $Ca_V2.3$(DSEE) mutant (ICa/IBa = 0.65 ± 0.02, n = 20; unpublished data). The $Ca_V2.3$(TSQN) mutant (square in Fig. 3, A and B), with no negative charges at the DCS, also had a smaller ICa/IBa ratio (0.44 ± 0.02, n = 11), but in this case the AMFE completely disappeared and the total current became a monotonic function of the Ca^{2+} mole fraction, without any marked minimum. Similar results were also found when the four residues of the DCS locus were mutated to alanine or glycine ($Ca_V2.3$(AAAA) or $Ca_V2.3$(GGGG) in Fig. 3), revealing important modifications in the energy profile of the channel pore (Hess and Tsien, 1984) clearly dependent upon the net charge carried by the residues at the DCS. Interestingly, the $Ca_V2.3$(DEEE) mutant with four charged residues at the DCS locus had an intermediate behavior, with a clear minimum in the current–mole fraction curve and an ICa/IBa ratio of 1.02 ± 0.05 (n = 15) between that of $Ca_V1.2$ and $Ca_V2.3$ (Fig. 3 B; see Discussion).

As a putative structural determinant of VGCC selectivity filter, mutations in the DCS locus are expected to modify permeation and single-channel conductance. In cell-attached patches performed in 100 mM Ba^{2+}, the single channel conductance of $Ca_V2.3$(DSED) (21 ± 1 pS, n = 9; Fig. 3 C) and $Ca_V2.3$(DSEE) (22 ± 1 pS, n = 7; not depicted) channels were clearly larger than the wild-type $Ca_V2.3$ (13 ± 1 pS, n = 8) and closely matched that of $Ca_V1.2$ channels (22 ± 2 pS, n = 8; Fig. 3 C) without any obvious changes in the channel open time (not depicted but see WT and mutated $Ca_V2.3$ current traces in Fig. 3 C). The $Ca_V2.3$(AAAA) single channel amplitude was on the other hand much smaller with only 4 ± 1 pS (n = 7). Our macroscopic recordings confirmed that, for the six mutated channels studied here, as for the others described below, the changes in selectivity occurred with no other modification in the biophysical properties of the channel, including current–voltage and steady-state inactivation curves (Fig. S3, A and B, and Tables S2 and S3). The kinetics of inactivation, estimated by the fractional current recorded at the end of a 2.5-s-long pulse (to +10 mV) in Ba^{2+} and in Ca^{2+}, were also not modified by these mutations (Fig. S3 C). Moreover, Cd^{2+} block of Ba^{2+} currents and current reversal potentials in 10 mM Ba^{2+} and 10 mM Ca^{2+} were only marginally affected (Table S1), demonstrating that mutations at the DCS have localized effects that did not spread through the protein via global perturbation of the channel gating, the pore structure, or the EEEE locus.

To challenge the idea that the DCS was involved in the specificity of the divalent cation selectivity profiles of HVA Ca^{2+} channels, we decided to switch the DCS of two related channels ($Ca_V2.1$ and $Ca_V2.3$) and analyze the selectivity profiles of the resulting channels.

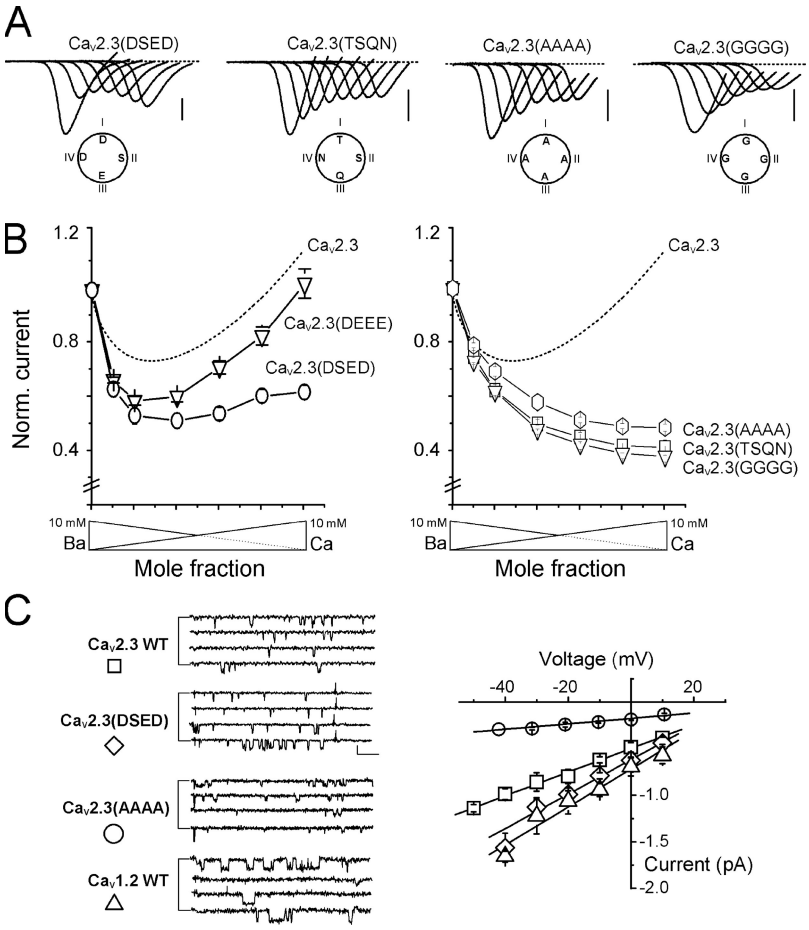

Figure 3. Mutations at the DCS locus suppress anomalous mole fraction of HVA. The four amino acids of the $Ca_V2.3$ DCS locus were mutated by adding or removing negatively charged residues. (A) Typical current traces recorded during voltage ramps under different ionic conditions (see Fig. 1) applied to oocytes expressing $Ca_V2.3$ channels with their DCS loci mutated in DSED (one negative charge added, $Ca_V2.3$(DSED)), DEEE (two negative charges added, $Ca_V2.3$(DEEE)), TSQN, AAAA, or GGGG (two negative charges removed, $Ca_V2.3$(TSQN), $Ca_V2.3$(AAAA) or $Ca_V2.3$ (GGGG)). (B) Current–mole fraction curves obtained for the above mutations. Right, effect of adding negative charges ($Ca_V2.3$(DSED), ○; $Ca_V2.3$ (DEEE), ▽). Left, effect of removing negative charges ($Ca_V2.3$(TSQN), □; $Ca_V2.3$ (AAAA), hexagone; $Ca_V2.3$ (GGGG), ▽). Note that the removal of the negative charges suppressed AMFE in all three cases. The dotted line represents the curve obtained with the WT $Ca_V2.3$ in Fig. 1. (C) Single-channel conductances of $Ca_V2.3$, $Ca_V2.3$(DSED), $Ca_V2.3$(AAAA), and $Ca_V1.2$ VGCC. Left, current traces in 100 mM $BaCl_2$ (pipette potential = +10 mV, except $Ca_V2.3$(AAAA) −20 mV). Right, current–voltage curves with superimposed linear regressions (13 ± 1 pS, 21 ± 1 pS, 4 ± 1 pS, and 22 ± 1 pS for $Ca_V2.3$, $Ca_V2.3$(DSED), $Ca_V2.3$(AAAA), and $Ca_V1.2$, respectively). Bar, 0.5 pA, 25 ms.

Currents recorded from oocytes expressing $Ca_V2.3$ (DEQN) mutated channels (with $Ca_V2.1$ DCS implemented in $Ca_V2.3$) displayed a strong AMFE, with a clear minimum recorded for small Ca^{2+} mole fractions and ICa/IBa ratio close to that of $Ca_V2.1$ channels (0.66 ± 0.02, n = 11). Conversely, currents recorded from oocytes expressing $Ca_V2.1$(TEQE) Ca^{2+} channels (with $Ca_V2.3$ DCS introduced in $Ca_V2.1$) displayed AMFE and IC/IBa ratio similar to those of $Ca_V2.3$ channels (ICa/IBa = 0.92 ± 0.02, n = 30, Fig. 4, A and B). Again, these modifications occurred without changes in the divalent over monovalent selectivity (Ca^{2+} or Ba^{2+} current reversal potentials were not modified, Fig. 4 C), and in the channel affinity for Cd^{2+}, the small differences in the EC50 for Cd^{2+} block between $Ca_V2.3$ and $Ca_V2.1$ being preserved (Fig. 4 C). Thus, mutations at the DCS locus only affected divalent selectivity without affecting the EEEE locus and EEEE-related properties (divalent/monovalent selectivity and Cd^{2+} binding site). These data suggested that DCS forms a distinct locus involved in the multi ionic nature of the channel selectivity filter (Kuo and Hess, 1993a,b).

To summarize the effects of these different HVA Ca^{2+} channel mutations on Ba^{2+}/Ca^{2+} selection, we have plotted the extent of AMFE (in arbitrary units, see methods) as a function of the number of negative charges at the DCS. AMFE values close to 1 indicate no mole fraction, while smaller values indicate the presence of stronger AMFE with larger Ca/Ba current ratios. As shown in Fig. 5, a clear and statistically significant relation between charges and AMFE exists (using the Spearman correlation test at a 0.05 level that makes no assumption on the nature of the relation). Although care should be taken in interpreting such a graph because AMFE and ICa/IBa ratios clearly do not vary linearly with ion binding energy (see Fig. 7); this nevertheless confirms the implication of the DCS locus on HVA channels selectivity.

It is worth noting that the conservation of the EEEE locus among HVA-VGCC does not exclude a crucial role in divalent selection but rather conservation of this role in the VGCC family. To test this idea, we mutated a nonconserved glycine residue on $Ca_V2.3$ that has been shown to slightly decrease Ca^{2+} binding at the EEEE locus and perturb channel permeation (Williamson and Sather, 1999) and analyzed the effects of this mutation on AMFE and Ca/Ba selectivity. The mutant $Ca_V2.3$ ($G_{1323}F$) channels displayed a decrease in AMFE and in relative Ca^{2+} currents (ICa/IBa) in close proportion with the reported decrease in the binding energy for divalent

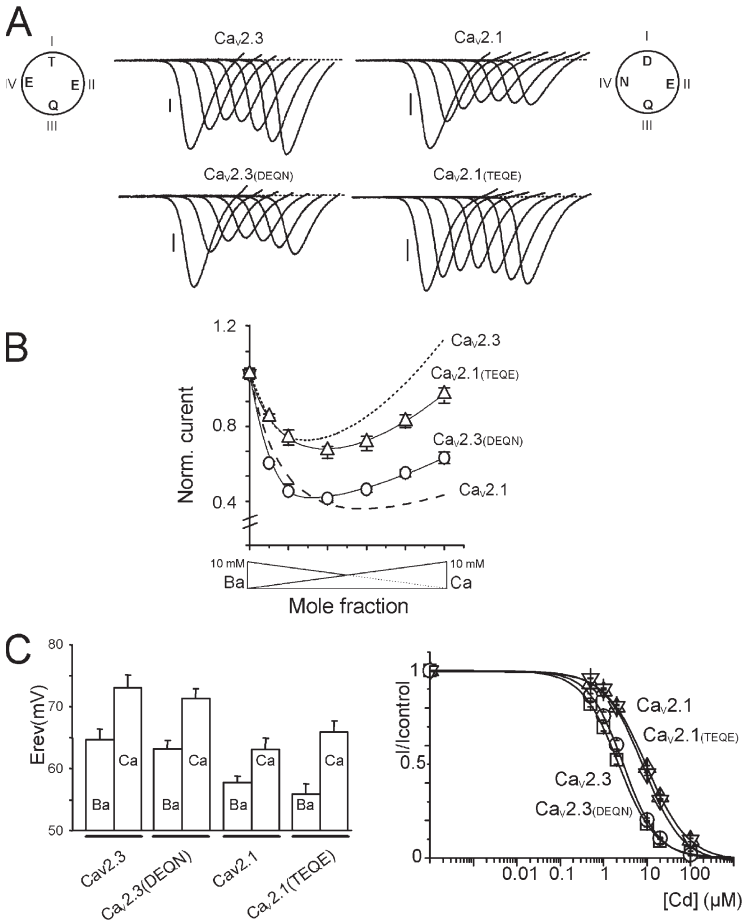

Figure 4. DCS locus controls the channel-specific cation selectivity profile. (A and B) A $Ca_V2.3$ channel with an engineered $Ca_V2.1$ DCS locus ($Ca_V2.3$(DEQN), square) displays AMFE and has an ICa/IBa ratio similar to $Ca_V2.1$. Conversely, a Ca2.1 channel with a $Ca_V2.3$ DCS locus ($Ca_V2.1$(TEQE), △) behaves like $Ca_V2.3$. (A) Current traces and (B) current–mole fraction curves. Dashed lines, current/mole fraction curves of parent channels, $Ca_V2.3$ and $Ca_V2.1$, determined in Fig. 1. (C) The current reversal potentials, recorded in 10 mM Ca^{2+} or 10 mM Ba^{2+} (left), and the Cd^{2+} block of Ba^{2+} current (right) for $Ca_V2.3$ (□) and $Ca_V2.1$(▽) channels are not changed by the mutations ($Ca_V2.3$(DEQN), ○; and $Ca_V2.1$(TEQE), △), suggesting the EEEE locus is not modified.

cation (Williamson and Sather, 1999) at the EEEE locus (ICa/IBa = 1.12 ± 0.03, n = 13 and 0.70 ± 0.05, n = 10 for CaV2.3 and $Ca_V2.3(G_{1323}F)$, respectively, Fig. S4, A and B), confirming the role of the EEEE locus in profiling channel permeation. On the other hand, mutation of a more distant nonconserved residue outside these two loci ($S_{1611}C$) had no effect either on $Ca_V2.3$ AMFE or on the relative Ca^{2+} currents (ICa/IBa = 1.12 ± 0.03, n = 13 and 1.06 ± 0.05, n = 6 for $Ca_V2.3$ and $Ca_V2.3$ ($S_{1611}C$), respectively, Fig. S4, A and B). This mutation had also no effect when made on the $Ca_V2.3$(DSED) mutant channels with ICa/IBa = 0.60 ± 0.05, n = 16 and ICa/IBa = 0.60 ± 0.08, n = 9 for $Ca_V2.3$(DSED) and $Ca_V2.3$(DSED)($S_{1611}C$).

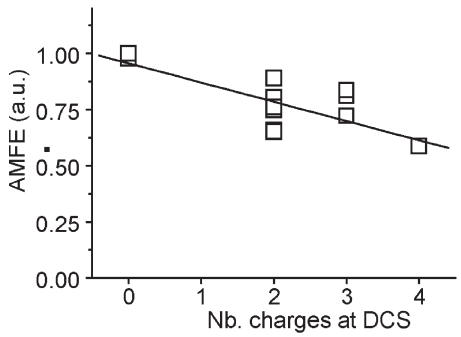

Figure 5. AMFE amplitude is correlated with the number of negative charges at the DCS. Scatterplot showing the amplitude of AMFE (calculated as the minimum of the current–mole fraction curve divided by the current in 10 mM Ca^{2+}) as a function of the number of negative charges for all the HVA mutations presented in this article.

Having in mind the large differences in the current–mole fraction curves between the different LVA channels, we have mutated the DCS locus of $Ca_V3.2$ (DCS: DVNG, see Fig. 6 A) to match that of either $Ca_V3.1$ or $Ca_V3.3$ (DCS locus: DKDG or EVNG, respectively), giving rise to the two mutated $Ca_V3.2$ channels: $Ca_V3.2$ (DKDG) and $Ca_V3.2$(EVNG). Current–mole fraction curves obtained with these three channels are displayed in Fig. 6 B, and clearly showed that the mutation of the $Ca_V3.2$ DCS to EVNG had no marked effect on AMFE and on the relative Ca^{2+} currents, while mutation to DKDG clearly modified these two parameters with the appearance of a small AMFE, absent in the parent $Ca_V3.2$ channels (curves of $Ca_V3.1$ and $Ca_V3.3$ channels are in dashed lines for comparison). As was the case for HVA channels, these changes appeared without any modification in the current–voltage and steady-state inactivation curves of the channels, the potential

of half-activation, the potential for half-inactivation, the slope of the two curves, and the reversal potential remaining unchanged (Fig. 6 C). The kinetics of the currents was also not modified (unpublished data). These data suggest that the modifications recorded with the $Ca_V3.2$(DKDG) mutant are not due to perturbations of the LVA EEDD locus, known to change reversal potential and current kinetics (Talavera et al., 2001, 2003).

Altogether, these results suggest that in HVA channels, the differences in divalent cation permeation recorded between voltage-gated Ca^{2+} channels were mainly due to variations in the structure of the DCS and EEEE loci, while in LVA channels, although these two sites are also implicated, they may not be the only determinants.

DISCUSSION

This first detailed analysis of the divalent cation selectivity of LVA and HVA VGCC identified a ring of nonconserved negative charges in the upper part of the pore directly involved in the selection of Ca^{2+} by Ca^{2+} channels. Modifications of the pattern of charged residues at this site affect both AMFE and relative Ca^{2+} current in HVA and LVA VGCC.

Previous work on $Ca_V1.2$ (Ellinor et al., 1995; Cibulsky and Sather, 2000; Sather and McCleskey, 2003) strongly suggested that high-affinity Ca^{2+} binding in the VGCC pore involved a single site, the EEEE locus. Although a role for the EEEE locus in divalent selection makes no doubt, its implication in the specificity of the selection observed here, via a global perturbation of the channel structure by DCS mutations, seems very unlikely for several reasons. First, the conservation of the pattern of charged residues at the EEEE/EEDD locus on HVA/LVA channels excludes this locus as a major determinant for channel-specific properties. Second, properties known to be strongly modified by mutation at the EEEE locus (Ba^{2+} or Ca^{2+} current reversal potentials, Cd^{2+} inhibition) are not changed by similar mutation at the DCS. Third, DCS mutations have no side effects on the voltage-dependent properties or on the current kinetics. On the other hand, we can speculate that quadruple mutations at internal EEEE locus (Ellinor et al., 1995; Cibulsky and Sather, 2000) may destabilize the less-conserved DCS locus and reduce Ca^{2+} binding at this site. Of course, our results on the $Ca_V2.3(G_{1323}F)$ mutant demonstrate that the EEEE locus participates at the global shaping of these permeation profiles, but not at their specificity encountered in the different VGCC.

We propose that the number of charged residues present at the VGCC DCS locus is critical for the binding of Ca^{2+} ions. Three negative charges are present in the $Ca_V1.2$ and $Ca_V2.3$(DSED) channels that display the highest Ba^{2+} conductance and the lowest ICa/IBa ratio. With only two negative charges, $Ca_V2.1$(DCS=DEQN),

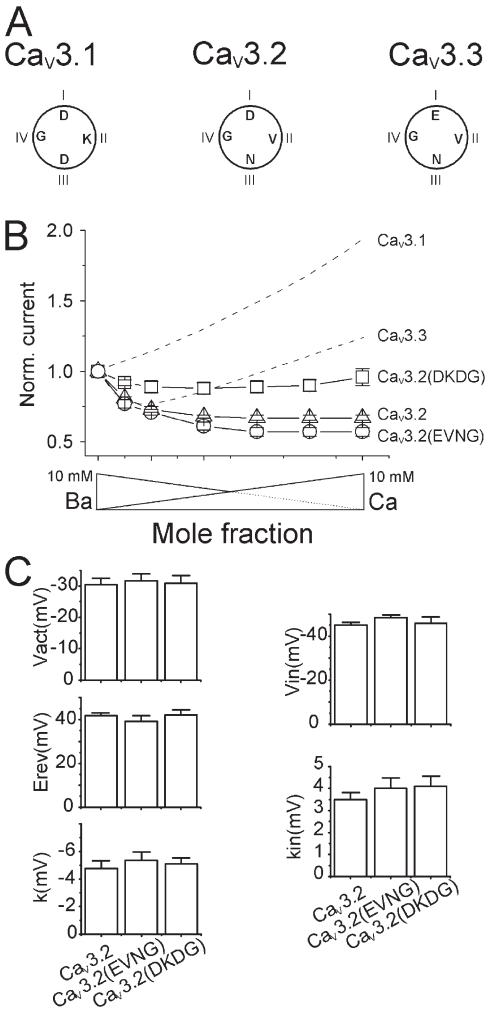

Figure 6. Mutations at the DCS locus modify selectivity profiles of LVA without changes in gating. (A) Schematic representation of the amino acids present at the $Ca_V3.1$, $Ca_V3.2$, and $Ca_V3.3$ DCS loci. (B) Current–mole fraction curves obtained for the WT (△) and two mutant $Ca_V3.2$ LVA channels mimicking the DCS loci of $Ca_V3.1$ ($Ca_V3.2$(DKDG), □) and $Ca_V3.3$ ($Ca_V3.2$(EVNG), ○). Ba/Ca current ratio was significantly changed for the $Ca_V3.2$(DKDG) mutant that also displayed a small AMFE as opposed to WT $Ca_V3.2$. (C) Voltage-dependent parameters of the current–voltage curves and inactivation curves of the $Ca_V3.2$, $Ca_V3.2$(EVNG), and $Ca_V3.2$(DKDG) LVA channels. These two mutations were without noticeable effects on these parameters.

$Ca_V2.2$ (DCS=DAME), and $Ca_V2.3$ (DCS=TEQE) have lower Ba^{2+} conductances but higher ICa/IBa ratios. The differences in the permeation profile that remain between these three channels may rely (a) on the noncharged residues present at this site (i.e., glutamines are known to be able to participate in Ca^{2+} binding; Kim et al., 1993), (b) on nonequivalent positioning of these two charges within the four channel domains and/or (c) on other neighboring amino acids that could finely shape the structure of the DCS. Although the characterization of the precise role of these three factors will require further experiments, it is worth noting that the effects of

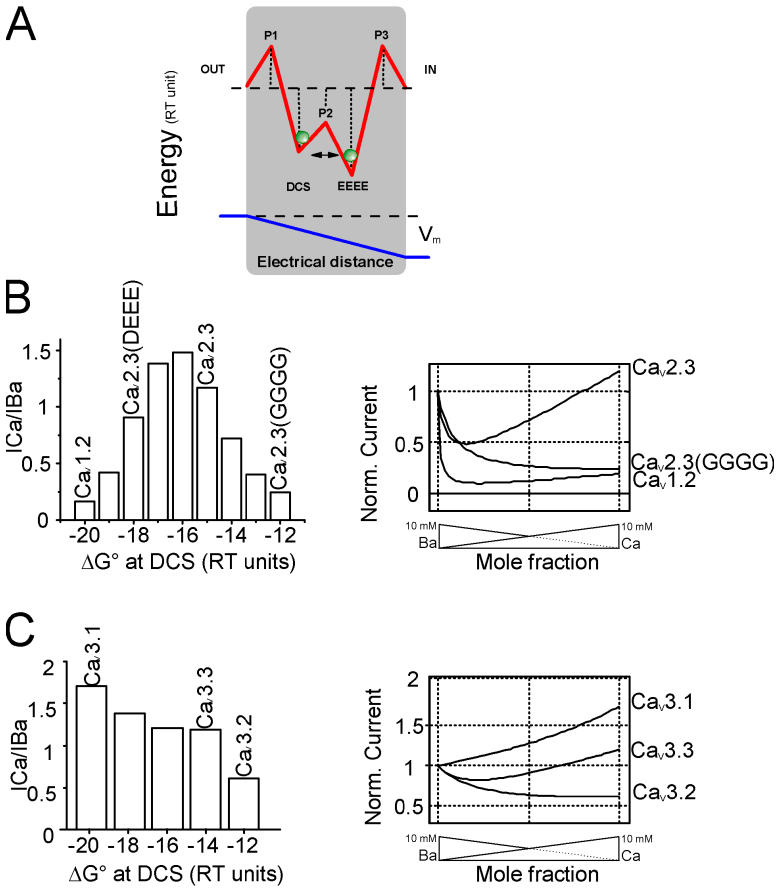

Figure 7. Numerical computation predicts mutant behavior. (A) Schematic representation of the energy profile used for computer modeling of the three barriers–two sites channel model. Barriers (P1, P2, P3) and wells (DCS and EEEE) are spaced equally (see Materials and methods). Membrane voltage drops across the narrow portion of the channel. (B, left) Simulated ICa/IBa ratios calculated for decreasing free energies at the external DCS locus of the $Ca_V2.3$ channel. The bell-shaped relation obtained for the DCS locus reached a maximum when DCS ΔG° equals the energy of the internal site. (B, right) Simulated current–mole fraction curves with three out of the four decreasing DCS ΔG° depicted on the left. These curves were labeled $Ca_V1.2$, $Ca_V2.3$(DEEE), and $Ca_V2.3$(GGGG), after comparison with original traces shown in Figs. 1 and 3, and suspected variations in free energy at DCS locus due to mutation. (C) Simulated ICa/IBa ratios calculated for decreasing free energies at the external DCS locus of the $Ca_V3.1$ channel. Energy profile of $Ca_V3.1$ was first adapted from $Ca_V2.3$ by adjusting the ΔG° at the EEEE locus considering that this locus in LVA channels (EEDD) has lower affinity for Ca^{2+}. Simulated current–mole fraction curves were then obtained by decreasing ΔG° at the DCS locus. Traces were labeled after comparison with original traces shown in Fig. 1 and suspected variations in free energy at DCS for the purpose of discussion.

the mutation of glutamate at the EEEE or EEDD loci in HVA and LVA channels are known to be strongly dependent on their location (Mikala et al., 1993; Talavera et al., 2001; Sather and McCleskey, 2003).

Different theoretical models have been proposed (Hess and Tsien, 1984; Miller, 1999; Roux, 1999; Sather and McCleskey, 2003) to account for the specific permeation properties of VGCC including (a) the selection of Ca over Na despite identical size and unfavorable concentration, (b) high Ca fluxes through open channels, and (c) high affinity block of monovalent currents by Ca^{2+}. In our case, we thought modeling the Ca^{2+} channel as a multi-ion single file pore with two Ca^{2+} binding sites and three energy barriers (Hess and Tsien, 1984) was particularly appropriate to understand the role of rings of negative charges in the channel lumen (Fig. 7 A). AMFE was computed using rate transitions calculated from Eyring rate theory with energy profiles for Ca^{2+} and Ba^{2+} derived from previous works (Hess and Tsien, 1984; Campbell et al., 1988). Current/mole fraction curves were obtained by sequentially decreasing the binding energy (ΔG°) of the external locus. For large ΔG° at the DCS (as expected for $Ca_V1.2$ channels), the ICa/IBa ratio was around 0.3 and total current showed AMFE with a strong reduction for small Ca^{2+} mole fractions (Fig. 7 B). When ΔG° was progressively decreased, keeping all other parameters constant, ICa/IBa reached a maximum at ∼1.5 (close to wild-type $Ca_V2.3$ channels) and then progressively returned to lower values. For these values, however, the current decreased monotonically and did not display AMFE (Fig. 7 B and Hess and Tsien, 1984) similar to recordings obtained from the $Ca_V2.3$(TSQN) $Ca_V2.3$ (AAAA) or the $Ca_V2.3$ (GGGG) channels without negative charges at the DCS. Whether one or multiple Ca^{2+} ions remain bound to the EEEE locus in these mutants devoid of AMFE is an open question that requires further experiments.

Our simulation also suggests that $Ca_V2.3$ (DEEE) mutant, with strong AMFE but ICa/IBa ratio close to the parent $Ca_V2.3$ channel, despite two additional negative charges at the DCS locus may result from DCS with a smaller ΔG° than $Ca_V1.2$ (Fig. 7 B). This can be explained by an increase in the electrostatic repulsion generated by the two additional carboxylates present on the DCS locus (Wu et al., 2000) leading to looser cation coordination. Mimicking the decrease in the ΔG° of the EEEE locus for the $Ca_V2.3(G_{1323}F)$ mutant (by 1 RT unit, see Williamson and Sather, 1999) also resulted in computed current–mole fraction curves (Fig. S4 B) close to those obtained experimentally in terms of relative Ca^{2+} currents and amplitude of AMFE. In an interesting alternative, the DCS locus could also constitute

one of the low affinity sites proposed by Dang and McCleskey (1998) to be necessary to overcome the large energy barriers flanking a single high affinity binding site. However, further experimental testing is required to more definitively validate one of these models.

In the case of LVA VGCC, simulation with decreasing ΔG° at the DCS (Fig. 7 C) and comparison with experimental results (Fig. 1) suggested the following sequence of ΔG° at DCS $Ca_V3.1 > Ca_V3.3 > Ca_V3.2$. Calculation of single channel currents using these differences in ΔG° gives a higher single channel conductance for $Ca_V3.3$ than for $Ca_V3.1$ or $Ca_V3.2$ (unpublished data), a situation that is recorded experimentally (Perez Reyes et al., 1998; Cribbs et al., 1998; Lee et al., 1999). However, although the DCS locus is undoubtedly involved in shaping the specific selectivity of LVA channels (see CaV3.2(DKDG) mutant), we were not able to completely restore the properties of the different CaV3 channels by mutation of the DCS. The existence of non-EEEE/EEDD structural determinants involved in the differences in the selectivity recorded between HVA and LVA and among LVA channels have been postulated by Talavera et al. (2001). Our results demonstrate that DCS is one of them and clearly suggest the existence of other elements, at least for LVA channels. The strong conservation of the EEDD locus and the P loop sequences in the different members of the LVA channel family locate these putative determinants implicated in LVA permeation at a more external position.

The presence of two sets of negative charges in the channel pore to regulate channel selectivity is a general scheme that has been conserved among different Ca^{2+} channels. A homologous external locus is also found in K_V (MacKinnon and Yellen, 1990; Crouzy et al., 2001) and Na_V channels (Hille, 2001) with important roles in permeation and pharmacology. From a physiological point of view, DCS clearly and directly participates in the generation of large Ca^{2+} influx (see Fig. 5). Its nonconservation among HVA channels plays a role in the definition of the channel-specific conductance, and thus could participate in the adaptation of each channel to its particular function: large and global Ca^{2+} influx for excitation–contraction coupling driven by $Ca_V1.2$, or smaller and more local Ca^{2+} changes required for $Ca_V2.1$-triggered synaptic transmission, for example. Our preliminary data, on $Ca_V2.1/Ca_V2.3$ and $Ca_V3.1/Ca_V3.2$ channels also suggest an implication in the differential block of these channels by external magnesium (unpublished data).

In conclusion, these results demonstrate the unexpected existence of an external locus that may form part of a structural context necessary for the pore of HVA and LVA Ca^{2+} channels to display high Ca^{2+} influx and specific divalent cation selectivity. Whether this site is also important for other pore-dependent properties such as toxin or drug binding is now under investigation.

The authors would like to thank Dr. M. Bellis for help with Matlab, Dr. T.P. Snutch (University of British Columbia, Vancouver, British Columbia, Canada) for providing the $Ca_V1.2$, $Ca_V2.1$, and $Ca_V2.3$ Ca^{2+} channel cDNA, Drs. E. Perez-Reyes (University of Virginia, Charlottesville, VA) and A. Monteil (IGH CNRS UMR 5203, Montpellier, France) for providing human $Ca_V3.1$, $Ca_V3.2$, and $Ca_V3.3$ cDNA, Drs. R. Dolmetsch, I. Findlay, I.A. Lefevre, R. MacKinnon, and G. Vassort for critical reading of the manuscript, and C. Delattre, J.M. Donnay, and J.C. Mazur for technical help.

This work was supported by CNRS, INSERM, Association Française contre les Myopathies, Association pour la Recherche contre le Cancer, Fondation pour la Recherche sur le Cerveau et Fondation Simone et Cino del Duca, and ANR N°Blan_06_01-148568.

Olaf S. Andersen served as editor.

Submitted: 1 March 2007
Accepted: 6 September 2007

REFERENCES

Almers, W., E.W. McCleskey, and P.T. Palade. 1984. A non-selective cation conductance in frog muscle membrane blocked by micromolar external calcium ions. *J. Physiol.* 353:565–583.

Begenisich, T.B., and M.D. Cahalan. 1980. Sodium channel permeation in squid axons. I: Reversal potential experiments. *J. Physiol.* 307:217–242.

Bourinet, E., Zamponi, G.W., Stea, A., Soong, T.W., Lewis, B.A., Jones, L.P., Yue, D.T., and Snutch, T.P. 1996. The α1E calcium channel exhibits permeation properties similar to low-voltage-activated calcium channels. *J. Neurosci.* 16:4983–4993.

Campbell, D.L., R.L. Rasmusson, and H.C. Strauss. 1988. Theoretical study of the voltage and concentration dependence of the anomalous mole fraction effect in single calcium channels. New insights into the characterization of multi-ion channels. *Biophys. J.* 54:945–954.

Catterall, W.A. 2000. Structure and regulation of voltage-gated Ca^{2+} channels. *Annu. Rev. Cell Dev. Biol.* 16:521–555.

Cibulsky, S.M., and W.A. Sather. 2000. The EEEE locus is the sole high-affinity Ca^{2+} binding structure in the pore of a voltage-gated Ca^{2+} channel: block by Ca^{2+} entering from the intracellular pore entrance. *J. Gen. Physiol.* 116:349–362.

Cibulsky, S.M., and W.A. Sather. 2003. Control of ion conduction in L-type Ca^{2+} channels by the concerted action of S5-6 regions. *Biophys. J.* 84:1709–1719.

Cloues, R.K., S.M. Cibulsky, and W.A. Sather. 2000. Ion interactions in the high-affinity binding locus of a voltage-gated Ca^{2+} channel. *J. Gen. Physiol.* 116:569–586.

Cribbs, L.L., J.H. Lee, J. Yang, J. Satin, Y. Zhang, A. Daud, J. Barclay, M.P. Williamson, M. Fox, M. Rees, and E. Perez Reyes. 1998. Cloning and characterization of alpha1H from human heart, a member of the T-type Ca^{2+} channel gene family. *Circ. Res.* 83:103–109.

Crouzy, S., S. Berneche, and B. Roux. 2001. Extracellular blockade of K^+ channels by TEA: results from molecular dynamics simulations of the KcsA channel. *J. Gen. Physiol.* 118:207–218.

Dang, T.X., and E.W. McCleskey. 1998. Ion channel selectivity through stepwise changes in binding affinity. *J. Gen. Physiol.* 111:185–193.

Dayring, H.E., A. Tramonato, S.R. Sprang, and R.J. Fletterick. 1986. Interactive program for visualization and modeling of proteins, nucleic acids and small molecules. *J. Mol. Graph.* 4:82–87.

Doyle, D.A., C.J. Morais, R.A. Pfuetzner, A. Kuo, J.M. Gulbis, S.L. Cohen, B.T. Chait, and R. MacKinnon. 1998. The structure of the potassium channel: molecular basis of K^+ conduction and selectivity. *Science.* 280:69–77.

Efimov, A.V. 1993. Standard structures in proteins. *Prog. Biophys. Mol. Biol.* 60:201–239.

Ellinor, P.T., J. Yang, W.A. Sather, J.F. Zhang, and R.W. Tsien. 1995. Ca^{2+} channel selectivity at a single locus for high-affinity Ca^{2+} interactions. *Neuron.* 15:1121–1132.

Feng, Z.P., J. Hamid, C. Doering, S.E. Jarvis, G.M. Bosey, E. Bourinet, T.P. Snutch, and G.W. Zamponi. 2001. Amino acid residues outside of the pore region contribute to N-type calcium channel permeation. *J. Biol. Chem.* 276:5726–5730.

Heinemann, S.H., H. Terlau, W. Stuhmer, K. Imoto, and S. Numa. 1992. Calcium channel characteristics conferred on the sodium channel by single mutations. *Nature.* 356:441–443.

Hess, P., and R.W. Tsien. 1984. Mechanism of ion permeation through calcium channels. *Nature.* 309:453–456.

Higgins, D.G., J.D. Thompson, and T.J. Gibson. 1996. Using CLUSTAL for multiple sequence alignments. *Methods Enzymol.* 266:383–402.

Hille, B. 2001. Ion channels of Excitable Membranes. Third edition. Sinauer Associates Inc., Sunderland, MA. 814 pp.

Isom, L.L., K.S. De Jongh, and W.A. Catterall. 1994. Auxiliary subunits of voltage-gated ion channels. *Neuron.* 12:1183–1194.

Jiang, Y., A. Lee, J. Chen, V. Ruta, M. Cadene, B.T. Chait, and R. MacKinnon. 2003. X-ray structure of a voltage-dependent K^+ channel. *Nature.* 423:33–41.

Kim, M.S., T. Morii, L.X. Sun, K. Imoto, and Y. Mori. 1993. Structural determinants of ion selectivity in brain calcium channel. *FEBS Lett.* 318:145–148.

Kuo, C.C., and P. Hess. 1993a. Characterization of the high-affinity Ca^{2+} binding sites in the L-type Ca^{2+} channel pore in rat phaeochromocytoma cells. *J. Physiol.* 466:657–682.

Kuo, C.C., and P. Hess. 1993b. Ion permeation through the L-type Ca^{2+} channel in rat phaeochromocytoma cells: two sets of ion binding sites in the pore. *J. Physiol.* 466:629–655.

Kurata, Y., R. Sato, I. Hisatome, and S. Imanishi. 1999. Mechanisms of cation permeation in cardiac sodium channel: description by dynamic pore model. *Biophys. J.* 77:1885–1904.

Lee, J.H., A.N. Daud, L.L. Cribbs, A.E. Lacerda, A. Pereverzev, U. Klockner, T. Schneider, and E. Perez-Reyes. 1999. Cloning and expression of a novel member of the low voltage-activated T- type calcium channel family. *J. Neurosci.* 19:1912–1921.

Lipkind, G.M., and H.A. Fozzard. 2001. Modeling of the outer vestibule and selectivity filter of the L-type Ca^{2+} channel. *Biochemistry.* 40:6786–6794.

MacKinnon, R., and G. Yellen. 1990. Mutations affecting TEA blockade and ion permeation in voltage-activated K^+ channels. *Science.* 250:276–279.

Mangoni, M.E., T. Cens, C. Dalle, J. Nargeot, and P. Charnet. 1997. Characterisation of α1A Ba^{2+}, Sr^{2+} and Ca^{2+} currents recorded with ancillary β1-4 subunits. *Receptors Channels.* 5:1–14.

Mikala, G., A. Bahinski, A. Yatani, S. Tang, and A. Schwartz. 1993. Differential contribution by conserved glutamate residues to an ion-selectivity site in the L-type Ca^{2+} channel pore. *FEBS Lett.* 335:265–269.

Miller, C. 1999. Ionic hopping defended. *J. Gen. Physiol.* 113:783–787.

Parent, L., and M. Gopalakrishnan. 1995. Glutamate substitution in repeat IV alters divalent and monovalent cation permeation in the heart Ca^{2+} channel. *Biophys. J.* 69:1801–1813.

Perez Reyes, E., L.L. Cribbs, A. Daud, A.E. Lacerda, J. Barclay, M.P. Williamson, M. Fox, M. Rees, and J.H. Lee. 1998. Molecular characterization of a neuronal low-voltage-activated T-type calcium channel. *Nature.* 391:896–900.

Rosenberg, R.L., and X.H. Chen. 1991. Characterization and localization of two ion-binding sites within the pore of cardiac L-type calcium channels. *J. Gen. Physiol.* 97:1207–1225.

Roux, B. 1999. Theories of ion permeation: a chaser. *J. Gen. Physiol.* 114:605–608.

Sather, W.A., and E.W. McCleskey. 2003. Permeation and selectivity in calcium channels. *Annu. Rev. Physiol.* 65:133–159.

Sather, W.A., J. Yang, and R.W. Tsien. 1994. Structural basis of ion channel permeation and selectivity. *Curr. Opin. Neurobiol.* 4:313–323.

Serrano, J.R., S.R. Dashti, E. Perez-Reyes, and S.W. Jones. 2000. Mg^{2+} block unmasks Ca^{2+}/Ba^{2+} selectivity of α1G T-type calcium channels. *Biophys. J.* 79:3052–3062.

Talavera, K., Staes, M., Janssens, A., Klugbauer, N., Droogmans, G., Hofmann, F., and Nilius, B. 2001. Aspartate residues of the EEDD pore locus control selectivity and permeation of the T-type Ca^{2+} channel α_{1G}. *J. Biol. Chem.* 276:45628–45635.

Talavera, K., A. Janssens, N. Klugbauer, G. Droogmans, and B. Nilius. 2003. Pore structure influences gating properties of the T-type Ca^{2+} channel α1G. *J. Gen. Physiol.* 121:529–540.

Tang, S., G. Mikala, A. Bahinski, A. Yatani, G. Varadi, and A. Schwartz. 1993. Molecular localization of ion selectivity sites within the pore of a human L-type cardiac calcium channel. *J. Biol. Chem.* 268:13026–13029.

Varadi, G., M. Strobeck, S. Koch, L. Caglioti, C. Zucchi, and G. Palyi. 1999. Molecular elements of ion permeation and selectivity within calcium channels. *Crit. Rev. Biochem. Mol. Biol.* 34:181–214.

Williamson, A.V., and W.A. Sather. 1999. Nonglutamate pore residues in ion selection and conduction in voltage-gated Ca^{2+} channels. *Biophys. J.* 77:2575–2589.

Wu, X.S., H.D. Edwards, and W.A. Sather. 2000. Side chain orientation in the selectivity filter of a voltage-gated Ca^{2+} channel. *J. Biol. Chem.* 275:31778–31785.

Yang, J., P.T. Ellinor, W.A. Sather, J.F. Zhang, and R.W. Tsien. 1993. Molecular determinants of Ca^{2+} selectivity and ion permeation in L-type Ca^{2+} channels. *Nature.* 366:158–161.